ORIGINAL ARTICLE

INTEGRATION OF LANDSAT IMAGERY AND HIGH RESOLUTION AEROMAGNETIC DATA FOR HYDROTHERMAL ALTERATION MAPPING IN PARTS OF THE MIDDLE-BENUE TROUGH, NIGERIA

| Adikwu Stephen Onum [1*] | Ibeneme Sabinus Ikechukwu [2] | Okereke Chikwendu Njoku[3] | Obioha Young Ezenwa [4] | and | Iduma Uche [5] |

[1,2,3,4] School of Physical Science | Federal University of Technology Owerri | Nigeria |
[5.] Kelma Geodynamic Limited Abuja | Nigeria |

| Received February 09, 2020 | | Accepted February 16, 2021 | | Published June 09, 2021 | | ID Article | Adikwu–Ref1-ajira090221 |

ABSTRACT

Background: The Middle Benue Trough is part of the Benue Trough that contained metal sulphides in the Cenomanian fractures of the Asu River Group. **Objective:** The objective of this study is to employ the use of Landsat 8 imagery and high resolution aeromagnetic data interpretation to delineate altered zones as well as demagnetized structures i.e structures that might have been altered magnetically due to the heat from hydrothermal fluid. **Methods:** The processing and analysis of the landsat-8 imagery was carried out using ArcGis and ENVI software by applying the Single Band Combinations, Band Ratio, Principal Component Analysis (PCA) and Reference Spectra Analysis. While Oasis montaj software was used in the interpretation of aeromagnetic data, in which enhancement filters such as reduction to equator, Analytical Signal, First Vertical Derivative (FVD), Upward Continuation and Tilt Derivative were utilized. **Results:** A composite using the bands 7, 5, 2 (RGB) highlighted areas with abundant iron oxides bearing minerals, and Clay minerals, as illite, kaolinite, and montmorillonite. The major anomalous alteration are seen at Gidan Shehu, east of Wukari, Kuka, Bambam, Uzam, Agor and minor anomalous alteration at Bangalala, Akwana and Dongwan. And, the high resolution aeromagnetic also shows that the structures trend majorly NE-SW and EW with minor NW-SE trends and show an indicative of lithology discrimination(magnetized and demagnetized areas) that correspond to the altered mapped area in the Landsate 8 Imagery. Results from the integration of Landsat 8 imagery and the high resolution aeromagnetic interpretation with the known geology suggest the existences of mineralized veins called the Lead-Zinc mineralization. **Conclusion:** Integrating Landsat 8 imagery with high resolution aeromagnetic interpretation and geological information defined Wukari, Akwana, Chonku, Fiyayi, Apar, Bangalala, Chindiya, Nafuche, Dampar, Kishr, Wuro Jam, Shinye, Yamere, Ibi, Ajikemai, Bembem, Gidan Tata and Jankaas area of highest potential of mineralization occurrences based on their geology, extensive alteration and structural complexity.The integrated technique adopted is effective in mineral exploration as it cover large area without any form of environmental degradation.

Keywords: *Delineate, Lithology, Anomalous, Structures and Enhancement.*

1. INTRODUCTION

Hydrothermal mineral deposits involve the movement of hot concentrated fluids deposited through faults (structures). Hydrothermal mineral deposit any concentration of metallic minerals resulting from the precipitation of solids from hot mineral-laden water (hydrothermal solution). The action of deeply circulating water heated by magma solutions are thought to have given rise to the hydrothermal solution. Energy released by radioactive decay or faulting of the Earth crust is also sources of heating that may be involved. The waters may precipitate their dissolved minerals in rocks openings or they may displace the rocks themselves to form so-called replacement deposits.

According to [1] the lead-zinc copper –barite deposits in the Benue Trough resulted from the hot basinal fluids leached metals from arkosic sediments and later precipitated them as metal sulphides in Cenomanian fractures of the Asu River Group. Detailed exploration to create proven mineral reserve database is a very expensive and risky investment, and thus is done systematically in stages. Such detailed exploration usually starts with a regional survey for magnetic, gravimetric or electromagnetic anomalies followed by ground truthing geological detailing. [2] pointed out the importanance of Landsat data for mineral exploration as it has a broad regional coverage with multispectral and multitiming features capable in indicating states, belts, mineralization areas and structures controlling mineralization like,contacts, linear and circular structures Aeromagnetic survey is also another important tool used in modern geological mapping and mineral exploration. The principle is similar to magnetic survey carried out with a hand-held magnetometer but enables larger areas coverage of the Earth's surface for regional reconnaissance; this is needed because the potential mineralized structures cover large area of land.

*Corresponding author Author & Copyright Author © 2021: |Adikwu Stephen Onum *|.

The main objective of this study is to employ the use of Landsat data and aeromagnetic data interpretation to delineate altered zones as well as demagnetized structures i.e structures that might have been altered magnetically due to the heat from hydrothermal fluid.

1.1 GEOLOGY OF THE STUDY AREA

The Benue Trough is approximately 1,000-km northeast-southwest trending intra-cratonic rift structure that extends from the northern limit of the Niger Delta to the southern margin of the Chad Basin and is partitioned geologically and geomorphologically into Lower, Middle, and Upper Benue Troughs(Figure 1). It is resting unconformably upon the Precambrian Basement of Nigeria. The Middle Benue is the near linear parts of the basin while the Lower Benue Trough, which shifts SW, includes two main structural units: the N6^{0}E trending Abakaliki Anticlinorium that is flanked by the Anambra Syncline trending N3^{0}E. Many models have been proposed for the origin of the Benue Trough [3,4,5,6,7,8,9,10,11,12]. All agreed that the origin of the Benue Trough is related to the continental separation of Africa and South America. The lithological units of the Middle Benue Trough have been detailed by [13]. The oldest sediments of the Middle Benue belong to the Asu River Group: A mixture of shale and siltstones of marine origin, and lava-flows, dykes, and sills overlie the Basement complex rocks. The youngest sediment is the Maastrichtian Lafia Formation.

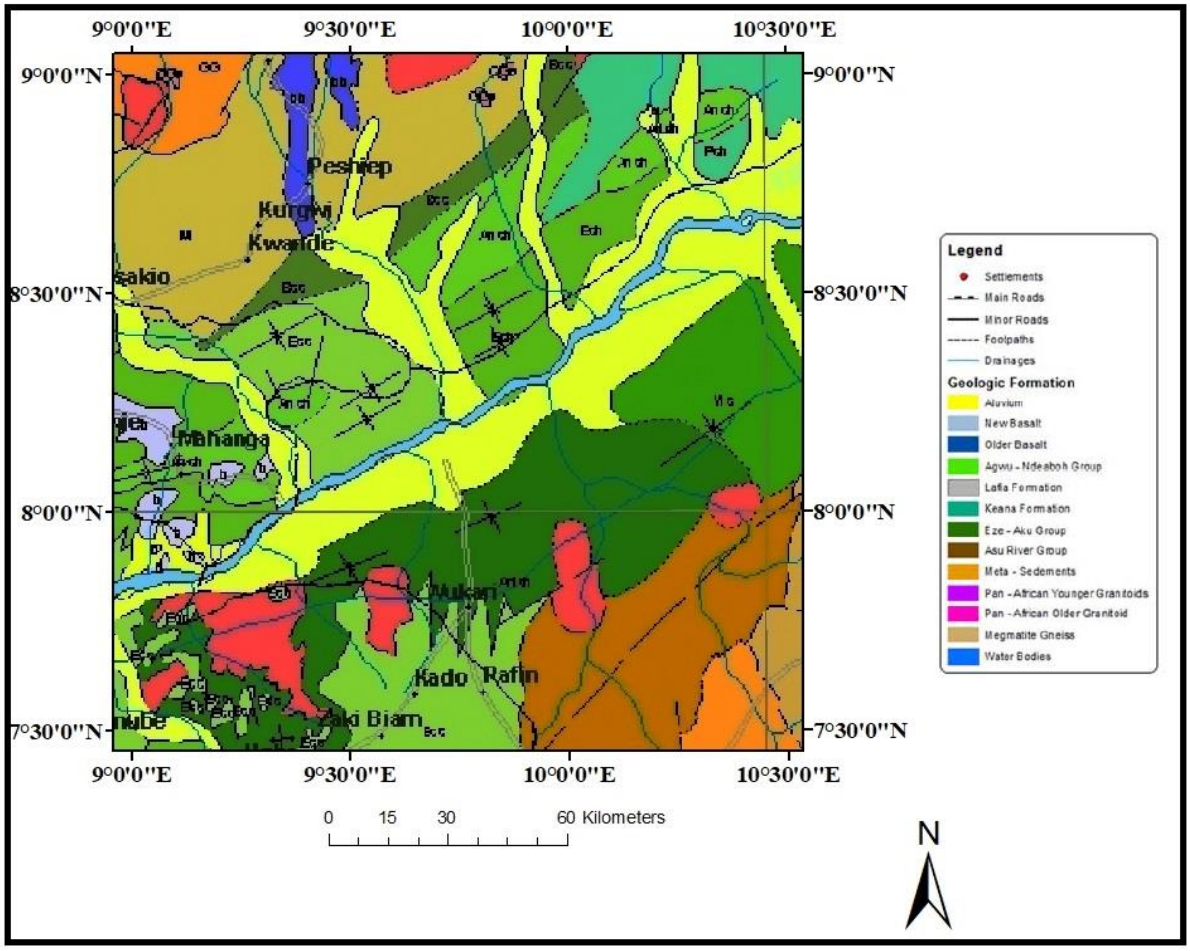

Figure 1: Geologic map of Central Benue Trough [14].

Previous geophysical work done within the study area [15,1617,18,19,20,21,22] dwelt more on the depth to basement and sediment thickness within the basin using source parameter imaging and Euler Deconvolution technique of aeromagnetic method and trend of structures. This work interpreted high-resolution aeromagnetic data with the aim of evaluating the complexity of sediments within the Central Benue Trough which has defined sediment thickness suitable for hydrocarbon generating by [18], [23], [21].

2. MATERIALS AND METHOD

2.1 Aeromagnetic Data Acquisition

The aeromagnetic dataset used for this study is from the high-resolution airborne survey coverage in Nigeria carried out by Fugro Airborne Survey at 826,000 along a series of NW – SE flight lines of magnetic surveys flown at 500 m line spacing and 80 m terrain clearance in 2009 and was obtained from the Nigerian Geological Survey Agency. The

parameter measured was the total magnetic field. The area coverage of about 27,225 km^2 and consists of nine (9) square blocks of map sheets (211, 212, 213, 232, 233, 234, 252, 253 and 253) of square block which represents a map on the scale of 1:600,000. The total magnetic intensity grid was generated using a minimum curvature algorithm. The digitized data were filtered using a low pass Fourier domain sub-routine filter to eliminate unwanted wavelengths and to pass longer wavelengths. Reduction-to-Equator (RTE) transformation was applied to the aeromagnetic data to minimize polarity effects. These effects are manifested as a shift of the main anomaly from the center of the magnetic source and are due to the vector nature of the measured magnetic field.

2.1.1 Data Processing and Enhancement

2.1.2 Regional - residual separation: Separation of regional and residual anomaly was done using Trend analysis in which a linear trend surface was fitted into the total aeromagnetic field data by a multiple regression technique for the purpose of removing the regional magnetic field. The linear surface fitted was removed from the regional component to obtain the residual magnetic anomaly map that was interpreted.

$$Total\ field = Regional\ field + Residual\ field \quad (1)$$
$$Residual\ field = Total\ field - fitted\ Surface/Regional \quad (2)$$

The Regional Field can be represented using the trend surface equation. Davies, (1973) expressed the regional field as;

$$Regional\ Field = a + bx_i + cy_j \quad (3)$$

Where, a, b and c are constants, x_i and y_j are coordinates in x and y directions.
Let Z_{ij} = the observed Total Field at ij^{th}data point.
Therefore,

$$Total\ Field\ (Z_{ij}) = (a + bx_i + cy_j) + Residual\ Field \quad (4)$$

Hence,

$$Residual\ Field = Z_{ij} - (a + bx_i + cy_j) \quad (5)$$

For a given magnetic data, the best fitting surface has the least square error,

$$fitting\ error = t - a - bx - cy \quad (6)$$

Where t is the magnetic value at x and y coordinate point.
Note that a, b and c are unknown coefficients while t, x and y are given. To obtain the least square error, the unknown coefficients a, b and c must yield zero first partial derivative.
Hence, the sum of the square of the fitting error becomes;

$$\sum_{i=1}^{N}\sum_{j=1}^{N}(fitting\ error)^2 = \sum_{i=1}^{N}\sum_{j=1}^{N}(t_{ij} - a - bx_i - cy_j)^2 \quad (7)$$

$where\ x_i, y_j\ and\ t_{ij}\ are\ vecctors\ and\ i\ and\ j\ are\ unit\ vector\ while\ t, x\ and\ y\ are$ Coefficient of the unit vector.

$$M = \sum_{i=1}^{N}\sum_{j=1}^{N}(t_{ij} - a - bx_i - cy_j)^2 \quad (8)$$

Taking the partial derivative of equation (9) with respect to a and equate it to zero,

$$\sum_{i=1}^{N}\sum_{j=1}^{N} t_{ij} - \sum_{i=1}^{N}\sum_{j=1}^{N} a - b\sum_{i=1}^{N}\sum_{j=1}^{N} x_i - c\sum_{i=1}^{N}\sum_{j=1}^{N} y_j = 0 \quad (9)$$

Partial derivative of the second constant b and equating it to zero;

$$\sum_{i=1}^{N}\sum_{j=1}^{N} t_{ij}\, x_i - a\sum_{i=1}^{N}\sum_{j=1}^{N} x_i - b\sum_{i=1}^{N}\sum_{j=1}^{N} x_i^2 - c\sum_{i=1}^{N}\sum_{j=1}^{N} x_i y_j = 0 \quad (10)$$

Taking the partial derivative of the third constant c;

$$\sum_{i=1}^{N}\sum_{j=1}^{N} t_{ij}\, y_j - a\sum_{i=1}^{N}\sum_{j=1}^{N} y_j - b\sum_{i=1}^{N}\sum_{j=1}^{N} x_i y_j - c\sum_{i=1}^{N}\sum_{j=1}^{N} y_j^2 = 0 \quad (11)$$

Solving this series of simultaneous equations will give the coefficients of the best fitting linear trend surface, being defined by the least-square criterion. The above equation can be written into matrix form as:

$$\begin{bmatrix} N & \sum_{i=1}^{N}\sum_{j=1}^{N} x_i & \sum_{i=1}^{N}\sum_{j=1}^{N} y_j \\ \sum_{i=1}^{N}\sum_{j=1}^{N} x_i & \sum_{i=1}^{N}\sum_{j=1}^{N} x_i^2 & \sum_{i=1}^{N}\sum_{j=1}^{N} x_i y_j \\ \sum_{i=1}^{N}\sum_{j=1}^{N} y_j & \sum_{i=1}^{N}\sum_{j=1}^{N} x_i y_j & \sum_{i=1}^{N}\sum_{j=1}^{N} y_i^2 \end{bmatrix} \begin{bmatrix} a \\ b \\ c \end{bmatrix} = \begin{bmatrix} \sum_{i=1}^{N}\sum_{j=1}^{N} t_{ij} \\ \sum_{i=1}^{N}\sum_{j=1}^{N} t_{ij} x_i \\ \sum_{i=1}^{N}\sum_{j=1}^{N} t_{ij} y_j \end{bmatrix} \quad (12)$$

The values of a, b, and c were obtained as follows;

$$\left.\begin{array}{l} a = 33293.2 \\ b = 3.5429 \\ c = -3.6132 \end{array}\right\} \quad (13)$$

The trend surface equation (regional gradient) becomes:

$$T(x,y) = 33213.2 + 3.472x - 3.5232\,y \quad (14)$$

Furthermore, the trend surface equation was then subtracted from the aeromagnetic (observed) data and the resultant residual anomaly was digitized.

2.1.3 Analytic signal filter: Nabighian suggested the concept of analytic signal (AS) and proposed that in the 2-D case, the horizontal and vertical derivatives of magnetic fields satisfy the Hilbert transform, thus can be regarded as analytic signals. The amplitude of the analytic signal is the same as the total gradient, independent of the direction of magnetization, and represents the envelope of both the vertical and horizontal derivatives over all possible directions of the earth's field and source magnetization [24] (Luo et al. 2011).

$$\frac{\partial T}{\partial z} = H\left[\frac{\partial T}{\partial x}\right] \quad (15)$$

Where;
T = Magnetic anomaly data.
H = Hilbert transform.

The analytical signal of a real signal f is defined as;

$$AS\left(\frac{\partial T}{\partial x}\right) = \frac{\partial T}{\partial x} - iH\left[\frac{\partial T}{\partial x}\right] \quad (16)$$

Where:

$i = -1$ [24]

According to the definition, the analytical signal of the potential field obtained by combining these two quantities into a two-dimensional quantity known as the analytic signal is given as;

$$\mathrm{AS(x,z)} = \frac{\partial T}{\partial x} + i\frac{\partial T}{\partial z} \quad (17)$$

Where:

$\frac{\partial T}{\partial x}$ and $\frac{\partial T}{\partial z}$ = Horizontal and vertical component of the total field respectively,
$T(x,z)$ = Magnitude of the total magnetic field
z and x = Cartesian coordinates for the vertical direction and the direction perpendicular to strike respectively
The amplitude of the analytic signal is defined as;

$$|\mathrm{AS(z)}| = \sqrt{\left(\frac{\partial T}{\partial x}\right)^2 + \left(\frac{\partial T}{\partial z}\right)^2} \quad (18)$$

The amplitude of the analytic signal is a symmetric bell-shaped function. By examining its profile across a magnetic source, the analytic signal can be used in interpretation to provide an indication of the edges of the causative body. Similarly, for the three dimensional case, the analytic signal is given by;

$$AS(x,y) = \left(\frac{\partial T}{\partial x}\right) + \left(\frac{\partial T}{\partial y}\right) + \left(i\frac{\partial T}{\partial z}\right) \quad (19)$$

Where its amplitude is defined as;

$$|AS(x,y)| = \sqrt{\left(\frac{\partial T}{\partial x}\right)^2 + \left(\frac{\partial T}{\partial y}\right)^2 \left(\frac{\partial T}{\partial z}\right)^2} \quad (20)$$

The maximum value of the analytic signal determines the edges of a magnetic body.

2.1.4 First Vertical Derivative: Derivatives (vertical) are based on the principle that the rates of change of magnetic field are sensitive to rock susceptibilities near the ground surface than at depth. First vertical derivative is physically equivalent to measuring the magnetic field simultaneously at two points vertically above each other, subtracting the data and dividing the result by the vertical spatial separation of the measurement points. The first vertical derivative was obtained from Laplace equation which is used to describe the magnetic potential field (U) thus,

$$\frac{\partial^2 \cup}{\partial x^2} + \frac{\partial^2 \cup}{\partial y^2} + \frac{\partial^2 \cup}{\partial z^2} = 0 \quad (24)$$

but, $-\text{grad} \cup = \text{T}$ (25)

Hence,

$$-\frac{\partial \text{T}}{\partial \text{x}} - \frac{\partial \text{T}}{\partial y} - \frac{\partial \text{T}}{\partial z} = 0 \quad (26)$$

Therefore,

$$\frac{\partial \text{T}}{\partial \text{z}} = -\left(\frac{\partial \text{T}}{\partial \text{x}} + \frac{\partial \text{T}}{\partial y}\right) \quad (27)$$

Where, $\cup = magnetic\ potential\ field$, $T = total\ magnetic\ field\ vector$

Rewriting equation (10) in numerical form we have,

$$-\frac{\partial T}{\partial x} = \left[\frac{T(x+\Delta x)-T(x)}{\Delta x} + 0(\Delta x)\right] \quad (28)$$

$$0(\Delta x) = error\ terms \quad (29)$$

$$-\frac{\partial T}{\partial x} = \left[\frac{T(x+\Delta x)-T(x)}{\Delta x}\right] \quad (30)$$

Similarly,

$$-\frac{\partial T}{\partial y} = \left[\frac{T(y+\Delta y)-T(y)}{\Delta y}\right] \quad (31)$$

Therefore,

$$\frac{\partial T}{\partial z} = -\left[\frac{T(x+\Delta x)-T(x)}{\Delta x}\right] - \left[\frac{T(y+\Delta y)-T(y)}{\Delta y}\right] \quad (32)$$

Equation (15) was applied on TMI grid to produce the first derivative map.

$$\Delta x = grid\ interval\ in\ x - direction$$
$$\Delta y = grid\ interval\ in\ y - direction$$

2.2 Remote Sensing Data Source

The Remote sensing data was obtained from the Earth Science Data Interface (ESDI) of the National Aeronautic and Space Agency (NASA). A Shuttle Radar Topographic Mission (SRTM) image of the same area was also obtained. To better interpretation the Landsat imagery was acquired at the peak of dry season. Single band combinations were applied in a first approach, in order to analyze the study area and visually interpret the multispectral imagery. For a preliminary geological study, a contrast-enhanced RGB combination (SWIR, NIR, and Visible) was created. The most contrasting band combination for lithological features and that provide more detail without additional enhancement should include one visible (2, 3 and 4), one NIR (5) and one SWIR (6 or 7) band [25,26]. Band Ratio Images enhancing hydrothermal altered rocks using band ratios with distinctive reflection features were produced. This corresponds directly to minerals associated with this alteration and represents surface expression for auriferous deposits. Thus, it was applied the ratio of Landsat 8 OLI band 4 over band 2, to highlight areas with abundant iron oxides bearing minerals, as brighter pixels. Vegetation density is a limiting factor when detecting and mapping hydrothermal altered rocks by band rationing. In order to minimize this limitation a spectral unmixing technique, as Principal Component Analysis, is applied. Firstly, this analysis was applied to the six Landsat 8 bands (2, 3, 4, 5, 6, and 7) that output an eigenvector matrix, represented in Table 1.

3. RESULT AND DISCUSSION

3.1 Landsat Imagery Analysis

3.1.1 Single Band Combinations: Using Landsat 8 OLI imagery, six bands (B2, B3, B4, B5, B6 and B7) were available to produce different band combinations, some of them enhancing relevant features for mineral exploration. A true colour image was produced with Landsat 8 visible bands 4, 3 and 2 (Red, Green and Blue, respectively) (Figure 3.1). With this band combination, it's possible to do an exploratory analysis of the area, identifying rock exposure areas (brown), vegetated areas (green), rivers and lakes (blue) and urbanized areas. In addition, some structural features such as faults and fractures were observed around Bangalala, Giden Shehu, Amar, Dongwan, Garkawa, Ajikemai, Kishr, Dampar, Kuka, Yamere, Shamankar, Bembem, Janka, Akiri, Yalwa, Shandam, JauroGarmaho, Adi, Apar, Hundu, Fiyayi, Kwana, Ugba, ZakiBiam, Sankara, Chonku, Wukari,Gidan Idi, Ngbebe, Donga, Avermun, Akume, Dooga, Gankol, Kurgwi, Kande and BakinChiwe.

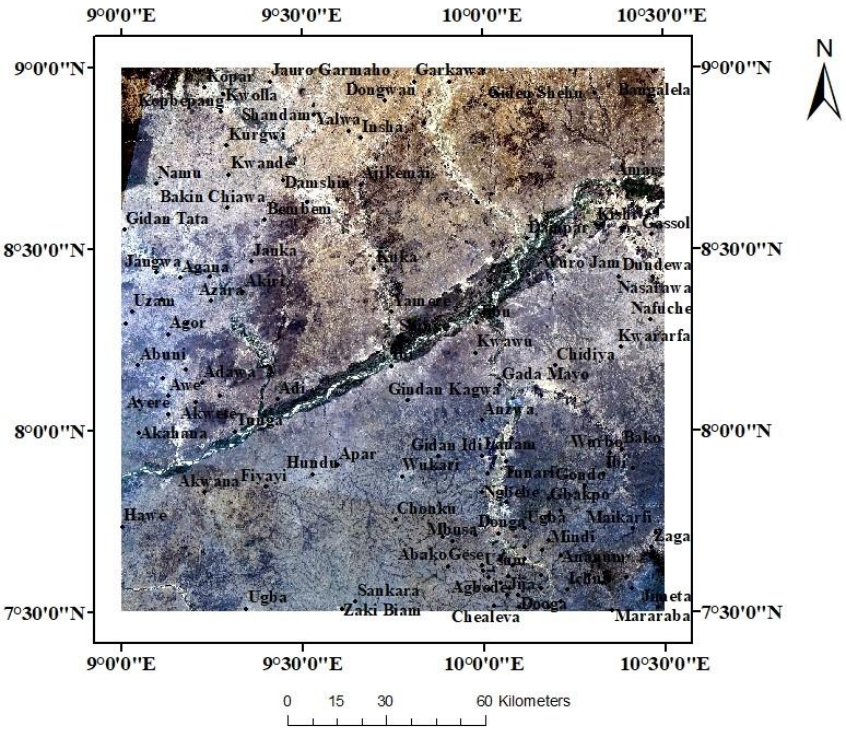

Figure 3.1: True Colour image. RGB combination of bands 4, 3, 2. Green colour represent vegetation, brown and brown represent soil or rock and blue water.

A False Colour image was created, using bands 5, 4 and 3 (R, G, B) (Figure 3.2). This band combination allows a better differentiation between vegetated areas (red areas) and good exposure outcrops (greyish colours). Light blue colour represents urbanized areas.

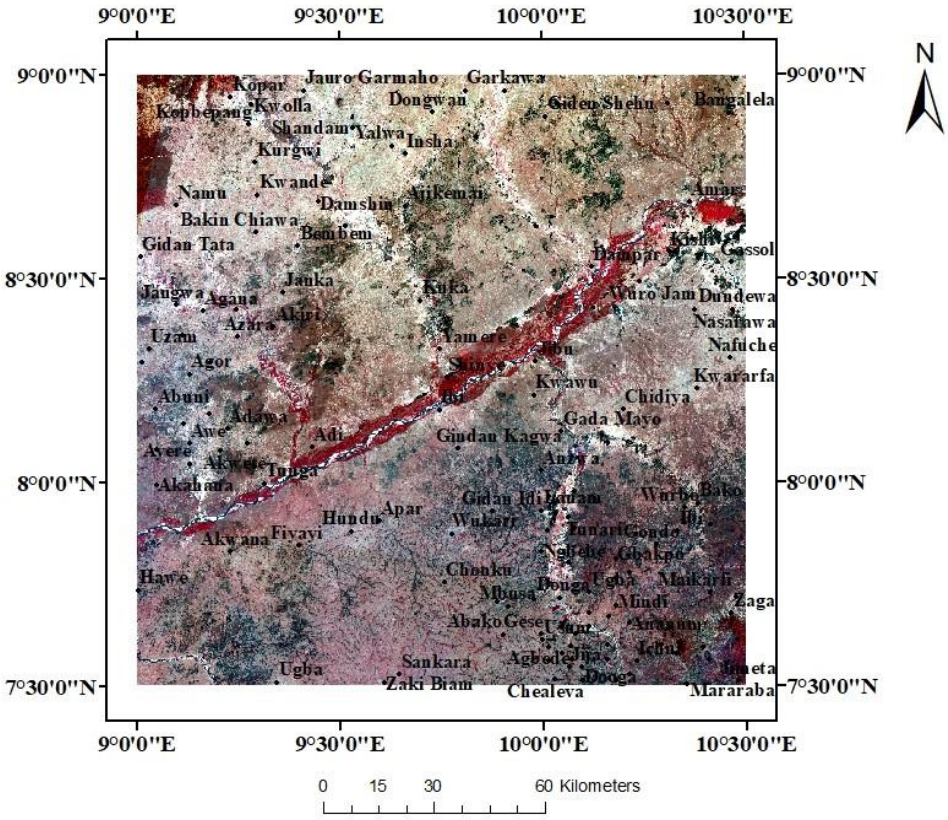

Figure 3.2: False Colour Composite. RGB combination of bands 5, 4, 3. Red colour represent vegetation, black represent water and rock or soil are represented by greyish colour. This RGB combination highlights the boundaries between vegetated and outcrop areas.

A composite using the bands 7, 5, 2 (RGB) was created (Figure 3.3) where it's possible identify outcrops as shades of orange and red, vegetation in light green and water in black.

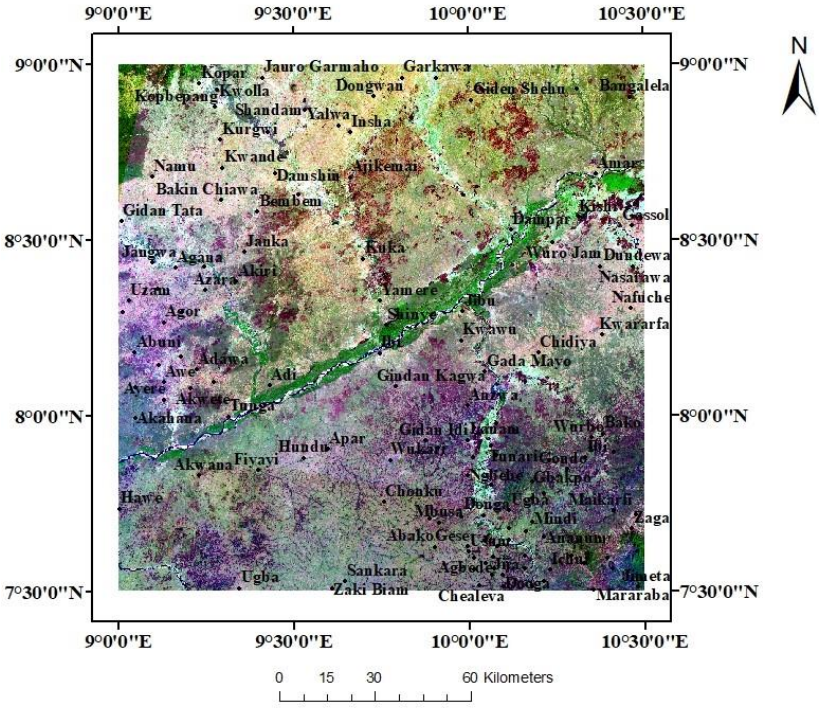

Figure 3.3: RGB combination for bands 7, 5, 2. Enhanced image where outcrops are represented in shades of orange and red, Vegetation in light green and water in black.

A band combination with a NIR band (band 5) and two SWIR bands (band 6 and band 7) was created, allowing a regional scale detection of geological features like faults, and differentiation of rock outcrops from vegetation (Figure 3.4). In this image, outcrops show a light blue colour, while vegetated areas an orange colour and water a black. Some hydrothermal alteration in outcrops areas can be identified as blue. The altered area is seen around Bangalala, Giden Shehu, Ajikeman. Kuka, Gessol, Akiri, Janka, Bembem, Wukari and Akwana.

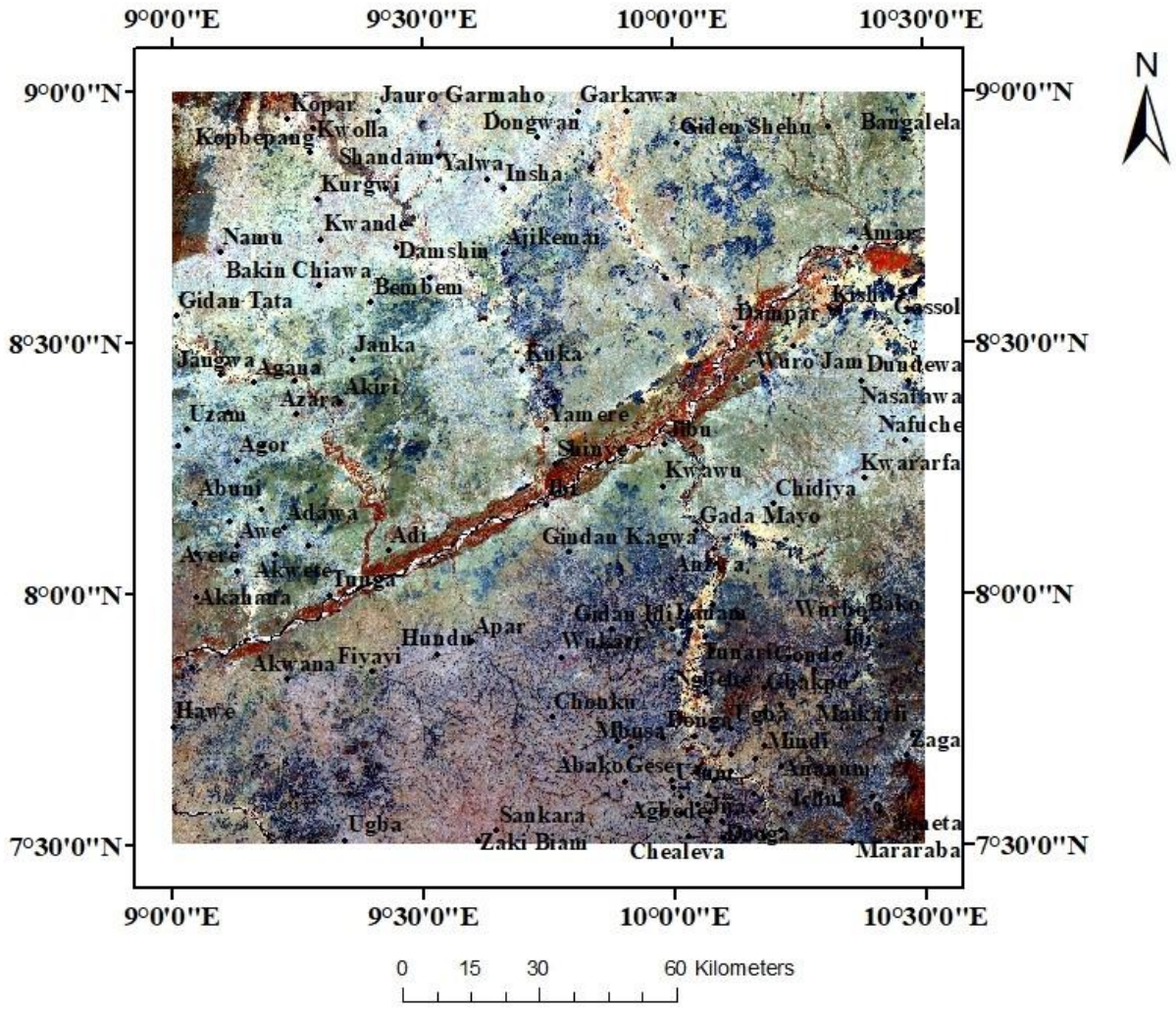

Figure 3.4: RGB combination for bands 5, 6, 7. In this image vegetated areas appear in orange colour, outcrops in light blue and water in black. Some hydrothermal altered rocks can be identified as blue.

3.1.2 Band Ratio

Thus, it was applied the ratio of Landsat 8 OLI band 4 over band 2, to highlight areas with abundant iron oxides bearing minerals, as brighter pixels (Figure 3.5)Ratio of Band 6 over band 5 discriminate ferrous minerals in bright tone (Figure 3.6). Clay minerals, as illite, kaolinite, and montmorillonite are discriminated with the ratio image of band 7 over band 5 as bright pixels (Figure 3.7). The ratio image of band 6 over band 7 distinguished altered rocks containing clays and alunite from unaltered rocks, where pixels are bright (Figure 3.8). pronounced alteration mapping interpreted by the occurrence of iron oxides bearing minerals as observed in ratio band 4 over band 5, Clay minerals, as illite, kaolinite, and montmorillonite in ratio of band 7 over band 5 and clays; and alunite in ratio of band 6 over band 7, indicted major anomalous alteration at Gidan Shehu, east of Wukari, Kuka, Bambam, Uzam, Agor and minor anomalous alteration at Bangalala, Akwana and Dongwan.

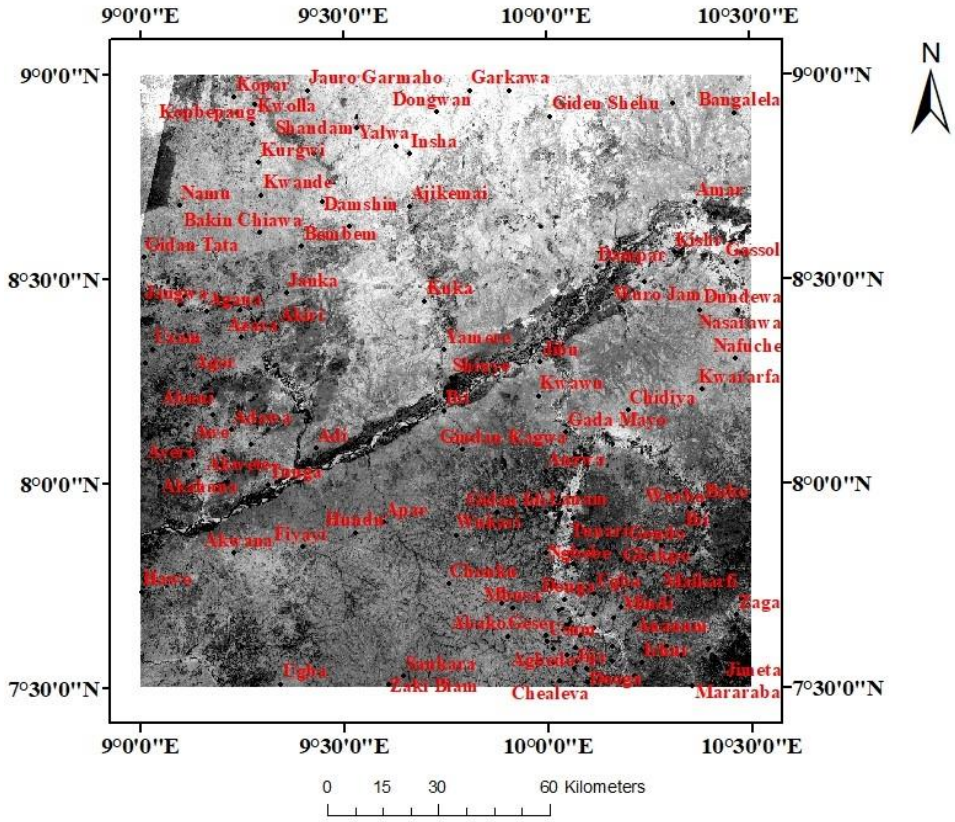

Figure 3.5: Landsat 8 band ratio 4/2 image reveals areas where iron minerals (hematite, goethite, limonite, etc.) are abundant shown in bright tones.

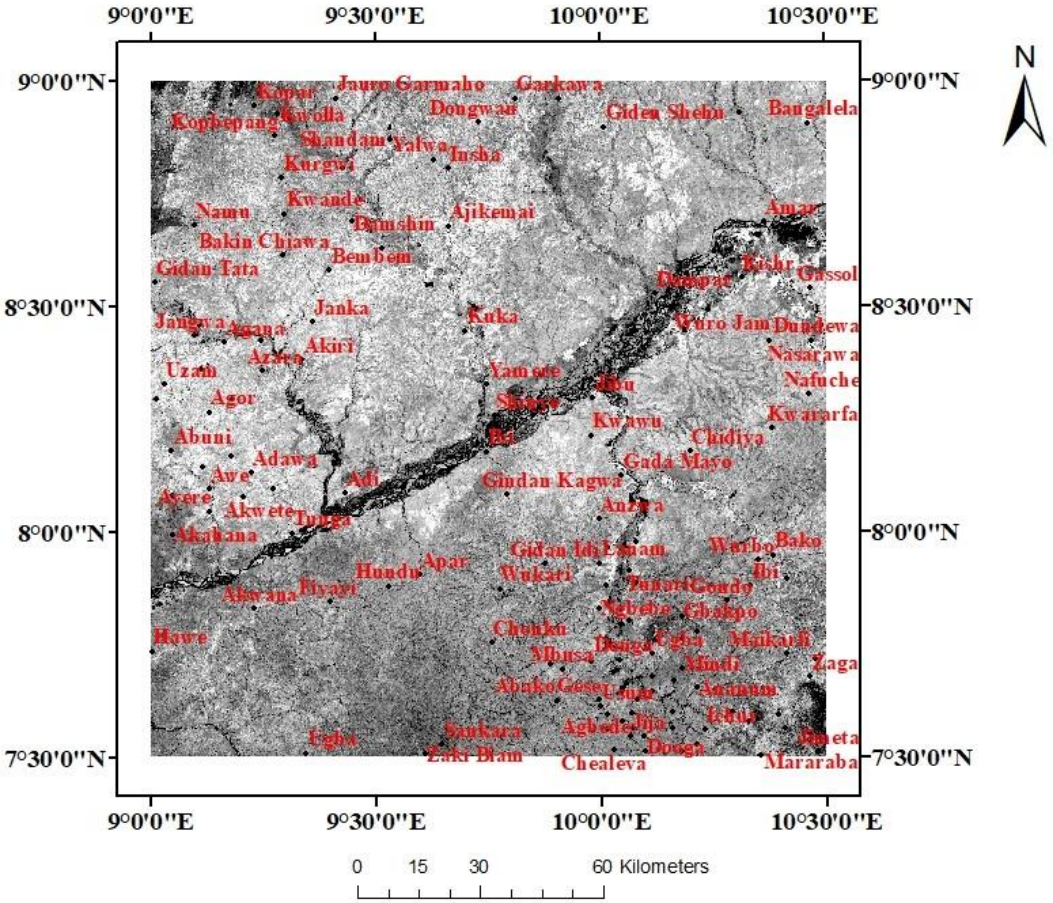

Figure 3.6: Landsat 8 band ratio 6/5 image discriminates ferrous minerals with bright tone.

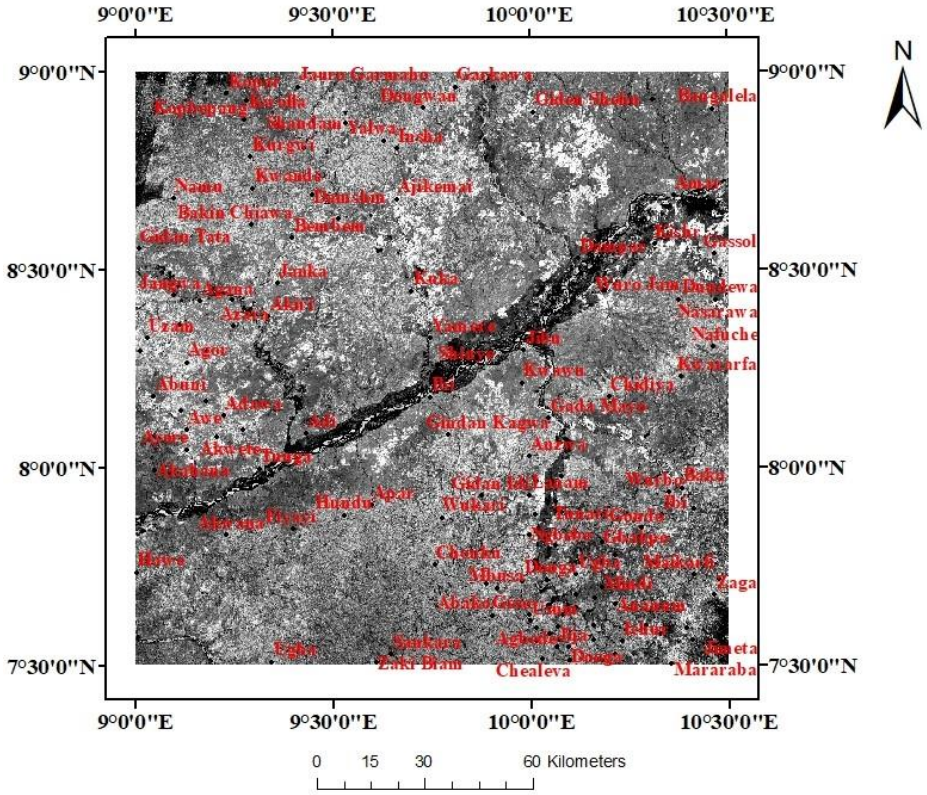

Figure 3.7: Landsat 8 band ratio (7/5) image reveals clay minerals, as illite, kaolinite and montmorillonite, in bright tones.

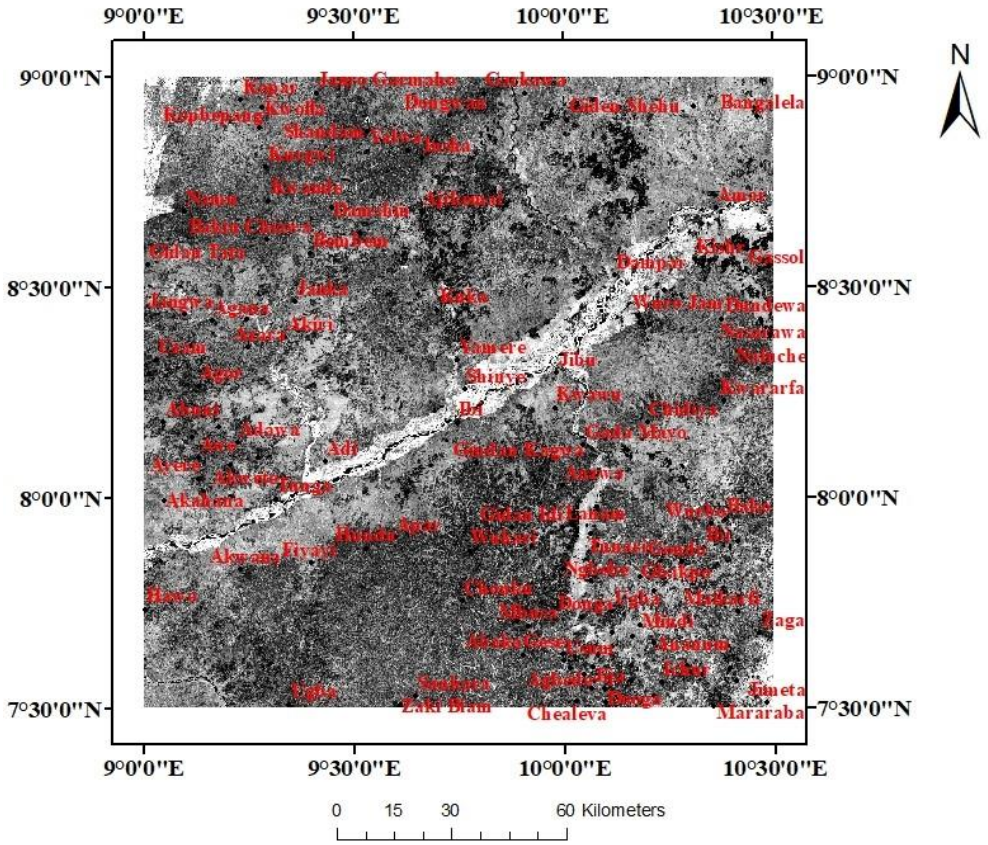

Figure 3.8: Landsat 8 band ratio 6/7 image shows alunite and hydrothermal clay minerals in bright tones.

An image incorporating these band ratios will discriminate altered from unaltered outcrop and highlight areas where concentration of these minerals occurs. An image using Sabin's ratio (4/2, 6/7 and 6/5 as RGB) was produced for lithological mapping and hydrothermal alteration zones (Figure 3.9). The ratio 4/2 was used for mapping iron oxides as hematite, limonite and jarosite, and has high reflectance in red region. The ratio 6/7 it's used to map clay minerals as kaolinite, illite and montmorillonite. The ratio 6/5 shows high reflectance in presence of ferrous minerals. In this Figure 4.9, light blue yellow colour represents outcrops and blue areas represent vegetation. Light green areas highlight hydrothermal alteration in outcrop rocks.

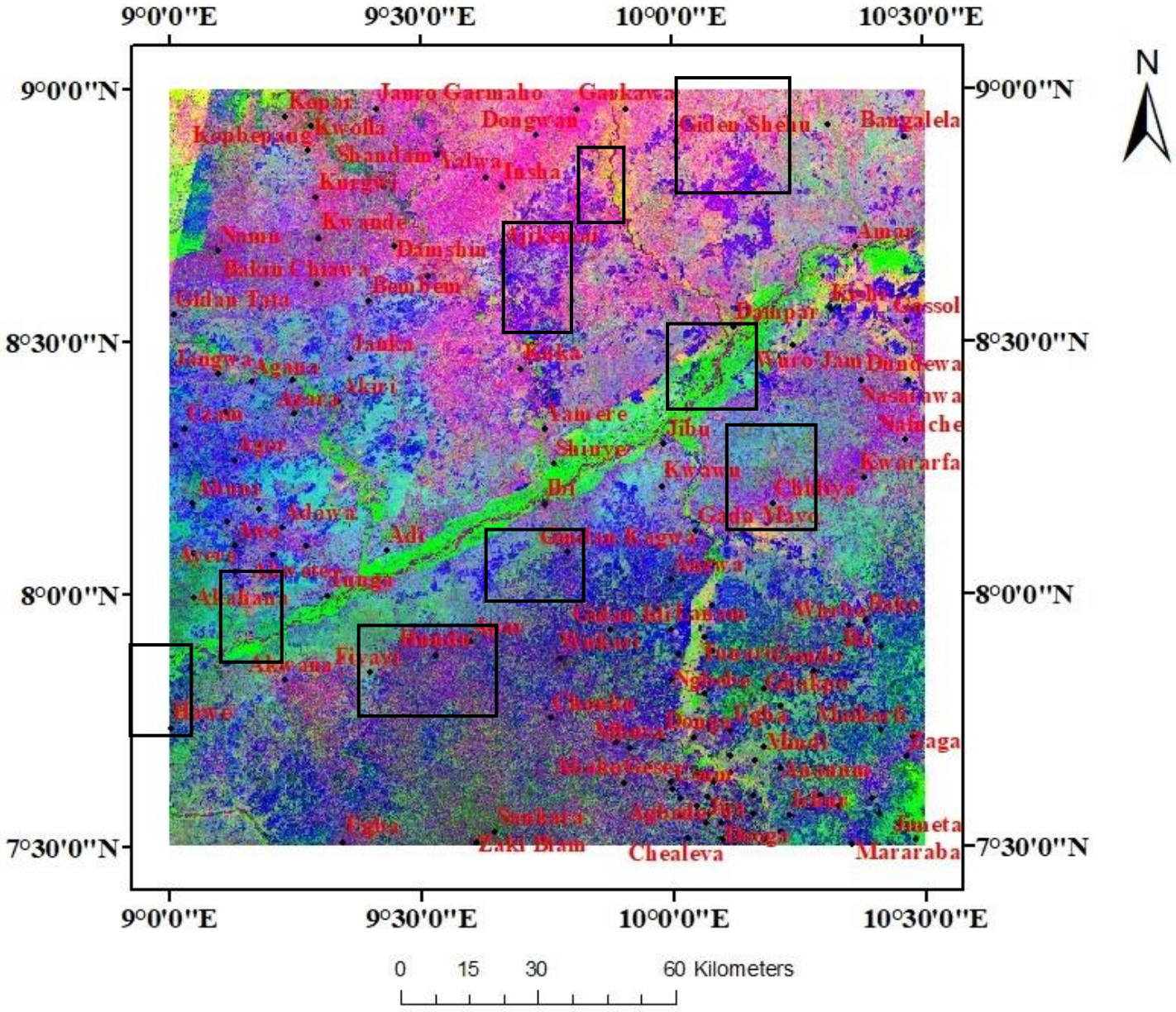

Figure 3.9: Sabin's ratio image (4/2, 6/7, 6/5). Outcrops are represented in light blue-yellow colour, vegetation in blue and water in dark green. Strong yellow represents buildings and other human constructions and light green altered rocks.

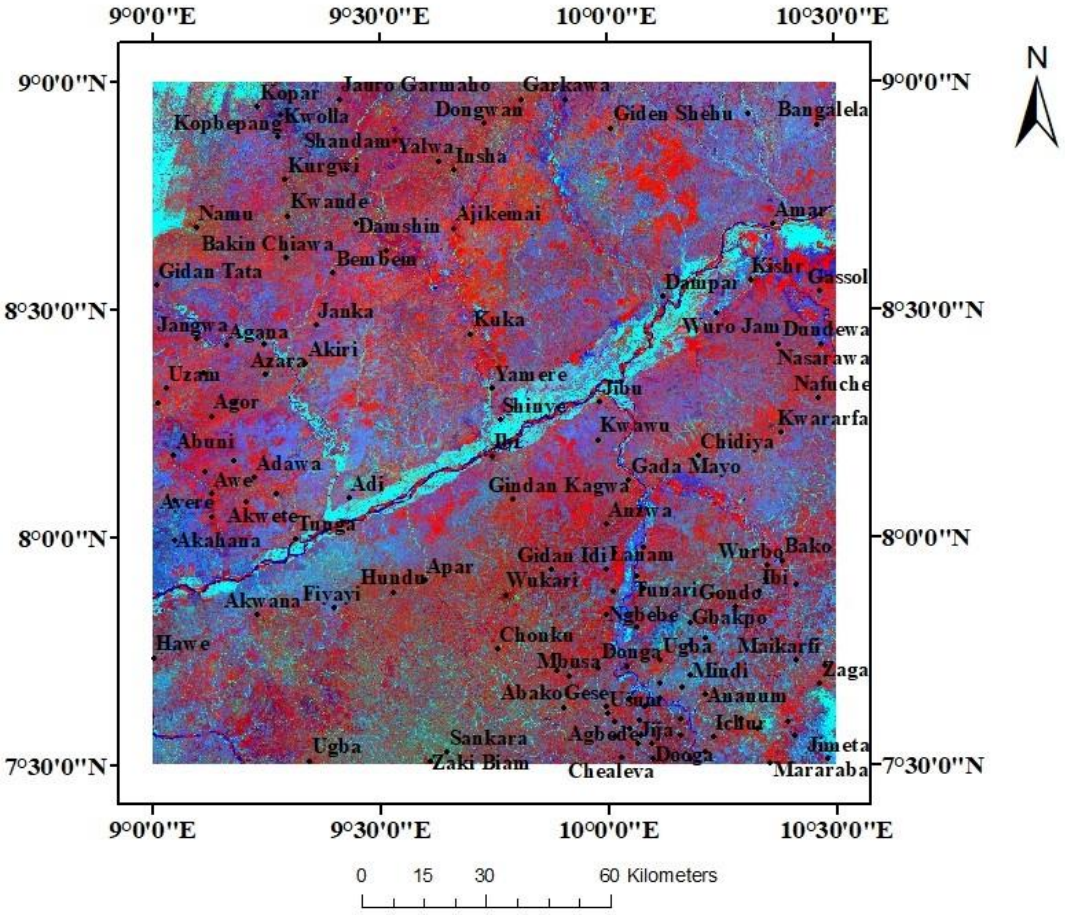

Figure 3.10: Kaufmann ratio (7/5, 5/4, 6/7). This band ratio combination highlight metasediments as dark green and granite outcrops are represented as rose, vegetation as light blue and water as red. Some red areas can be related to the hydrothermal alteration.

3.1.3 Principal Component Analysis (PCA)

This analysis was applied to the six Landsat 8 bands (2, 3, 4, 5, 6, and 7) that output an eigenvector matrix, represented in Table 1. This result allowed identifying which PC contains more useful spectral information from Landsat 8 bands which has much higher contrast than the original bands.

Table 1: Eigenvectors and eigenvalues of PCA on Landsat 8 imagery.

	PC1	PC2	PC3	PC4	PC5	PC6
BAND 2	0.33541	0.44101	0.47773	-0.53674	0.17977	-0.37997
BAND 3	0.32237	0.31849	0.27952	0.08211	-0.11697	0.83432
BAND 4	0.30589	0.34953	0.05763	0.66891	-0.42059	-0.39573
BAND 5	0.60051	-0.73032	0.29534	0.10042	0.07808	-0.05112
BAND 6	0.45833	0.01101	-0.63896	-0.43077	-0.44251	0.01313
BAND 7	0.34545	0.22004	-0.44139	0.24917	0.75841	0.01221
EIGENVALUES	0.06686	0.00279	0.00102	0.00004	0.00002	0
PERCENTOFEIGENVALUES	**94.5305**	**3.9425**	**1.4443**	**0.0549**	**0.0227**	**0.0051**
ACCUMULATIVE OFEIGENVALUES	94.5305	98.473	99.9173	99.9722	99.9949	100

The sign and magnitude of eigenvector loadings in each PC correspond to the spectral properties of surface materials such as rock, vegetation, and soils [27].

PC1 explains 94.5% of the total variance of the data, as shown in table 1. This PC is composed of positive values of all 6 bands and is being responsible for the overall scene brightness. PC2 contains 3.9% of the original data variance and PC3 represents just 1.4%. The firsts three PC that contain the most data variance was combined in an RGB composite (Figure 3.11) and it is useful for lithological mapping purposes. Green-yellow colours represents granite outcrops, while blue colour represent metasediments; purple represent vegetation and light blue water bodies. Light green areas highlight hydrothermally altered rocks.

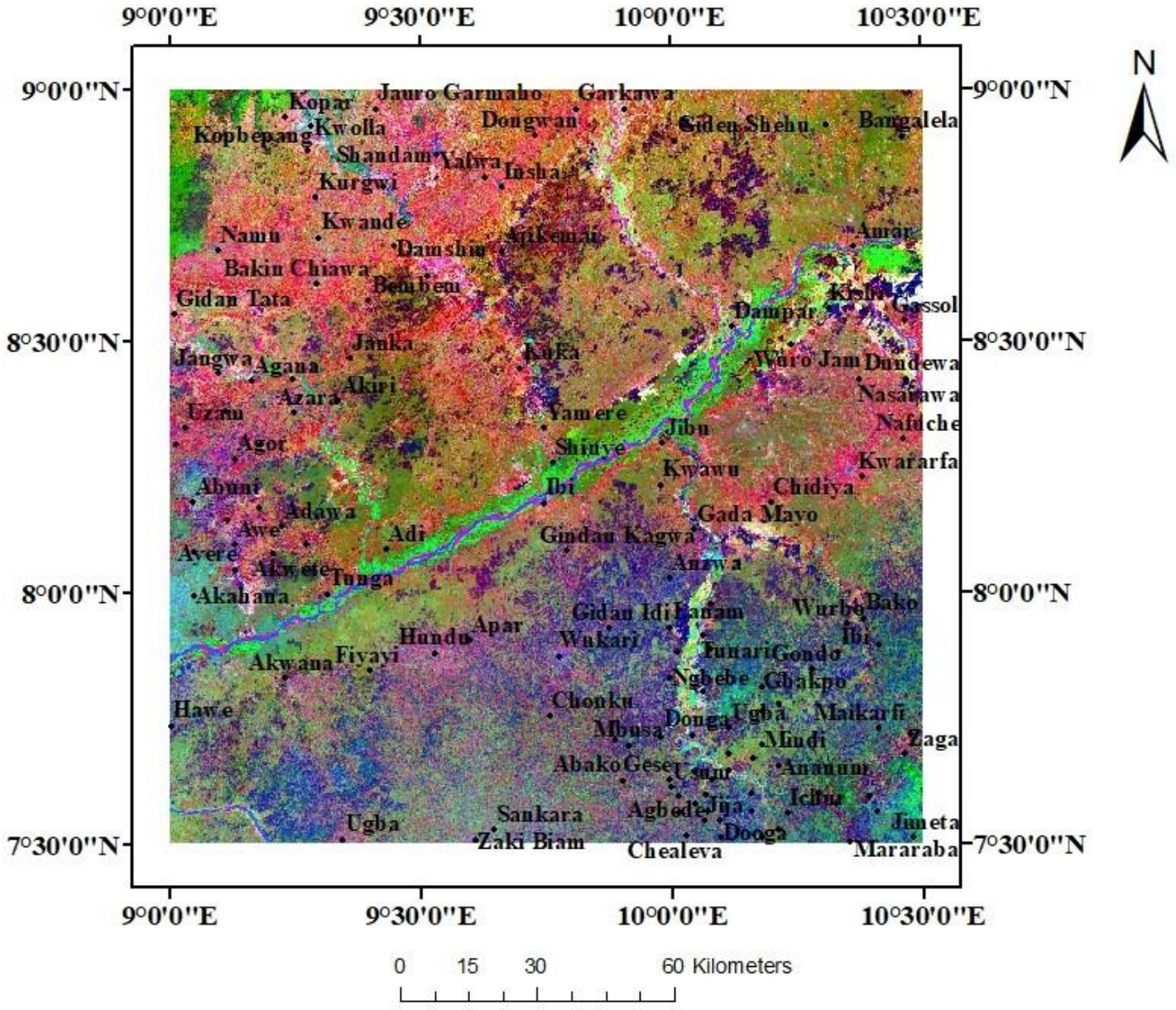

Figure 3.11: RGB colour combination of Principal Component Analysis 1, 2, 3 components. Green-yellow colours represent outcrops, vegetation in purple, water as light blue and metasediments as blue.

From the Landsat analysis, an alteration map (figure 3.11) was produce. The alteration map represents the map of thermally altered rocks within the Middle Benue Trough.

3.2 Aeromagnetic interpretation

3.2.1 Total Magnetic Intensity (TMI) Map: The total magnetic field intensity map is presented as total field intensity. From these figures, magnetic anomalies both short and long wavelengths were interpreted within the study area. These interpreted anomalies are represented by magnetic highs and lows respectively.

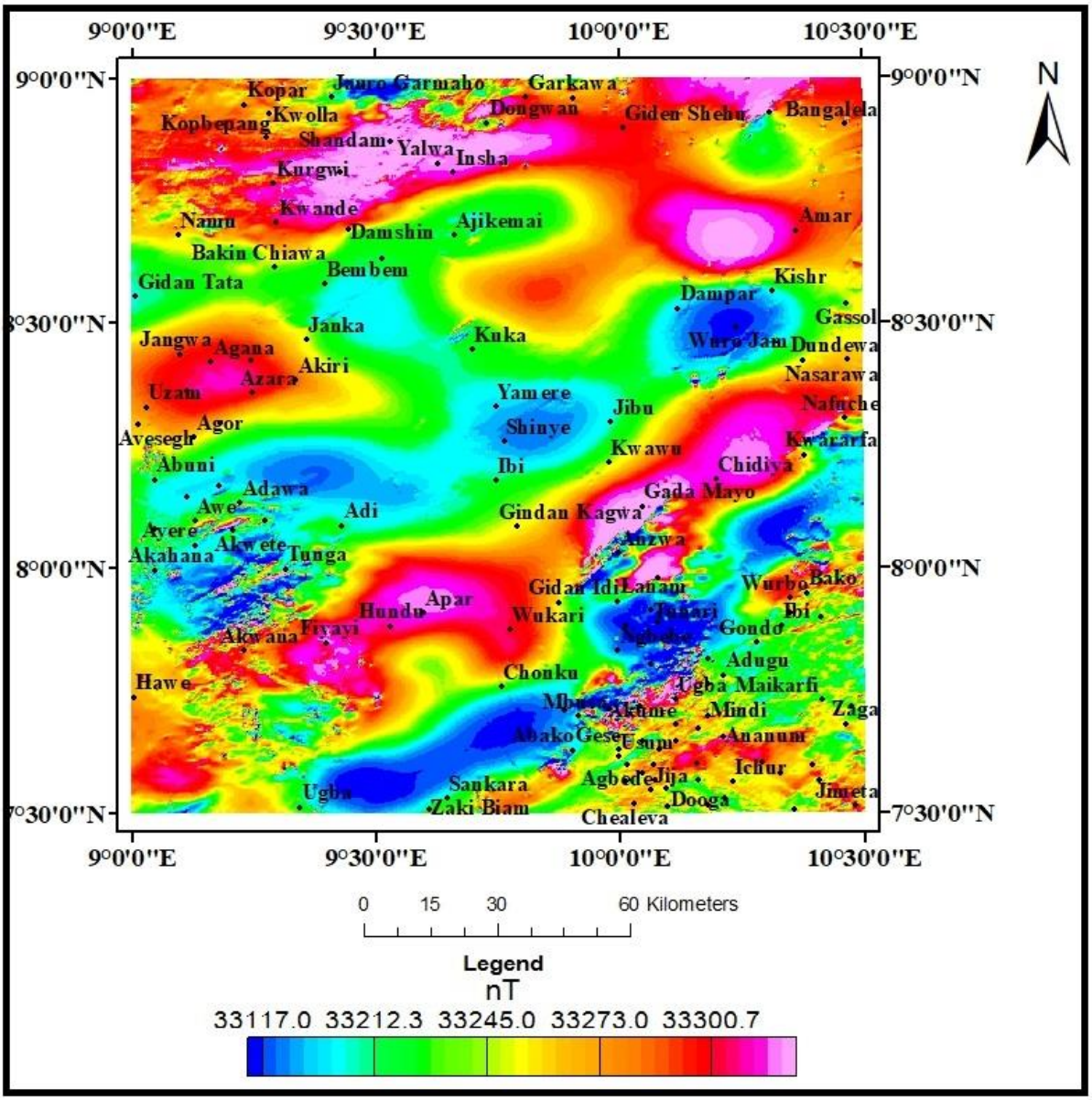

Figure 3.12: Total Magnetic Intensity, RMI grid map.

The residual magnetic intensity (RMI) map (Figure 3.13) emphasizes the intensity and the wavelengths of local anomalies. The rock formations at low magnetic latitude are magnetized parallel to the Earth's magnetic field; the area around Kopar, Jauro Garmaho, Peshiep, Kopbepand, Kurgwi, Shandam, Yalwa, Kwande and Namu is characterized by high magnetic susceptibility and short wavelength anomalies, this signature is commonly associated with basement rocks. Anzwa, Ugba, Zaki Biam, Sankara, Chonku, Ngbebe, Toskundi, Tunari, Bayawal and Nwarara are characterized by low magnetic susceptibility and both long and short wavelength anomalies. Donga, Mbusa, Abako Avermum, Sankara, Dooga, Norjjo Gankoi, and Zaga is characterized moderate magnetic susceptibility and short wavelength anomalies. Akwana and Fiyayi is also characterized by high magnetic susceptibility bodies and short wavelength anomalies, while nearby Hawe, Hundu, Apar, Wukari and Chonku is characterized by high magnetic susceptibility and long wavelength anomalies. A NE-SW trending low magnetic susceptibility is overserved at Akahana, Tunga, Keffin, Awe, Adawa, Amafan through Ibi, Shinye, Yamere to Dampar, Kishr, Wuro Jam; Gassol. Bangalala and Giden Shehu is characterized by both long and short wavelength with high magnetic susceptibility, while Gidan Tata, Bakin Chiawa, Bembem, Shamanajar and Ajikemai is characterized by moderate to low magnetic susceptibility.

Gidan Tata, Bakin Chiawa, Bembem, Shamanajar and Ajikemai are interpreted to be area sedimentary environment that has undergone mobilization of magnetic minerals such as magnetite and hematite. Akahana, Tunga, Keffin, Awe, Adawa, Amafan through Ibi, Shinye, Yamere to Dampar, Kishr, Wuro Jam and Gassol. Bangalala and Giden Shehu are interpreted to be area of igneous intrusive rocks that has undergone tectonism leding to the destruction of magnetic minerals and emplacement of intrusive rocks. Akwana, Fiyayi Hawe, Hundu, Apar, Wukari and Chonku are interpreted as areas of intense structural activities with intrusive rocks and occurrence of feroginized sandstone; Hawe, Hundu, Apar, Wukari and Chonku has thicker sedimentary cover when compared to Akwana and Fiyayi Hawe. The NE-SW stretching low magnetic amplitude is interpreted as Akahana, Tunga, Keffin, Awe, Adawa, Amafan through Ibi, Shinye, Yamere to Dampar, Kishr, Wuro Jam and Gassol. Bangalala and Giden Shehu are interpreted as zone of thick sediment cover is high faulting and fracturing and thermal activities during the santonian orogeny. Kopar, Jauro Garmaho, Peshiep, Kopbepand, Kurgwi, Shandam, Yalwa, Kwande and Namu are interpreted to be zone of igneous environment (Basement Complex). Jangwa, Agana, Madakin, Azaza, Gidan Shahu and Bangalala and Akiri is interpreted to be areas of thick sediment cover and feroginized sandstone, but Gindan Shehu and Bangalala is interpreted to as having shallow magnetic sources and intense fracturing and faulting.

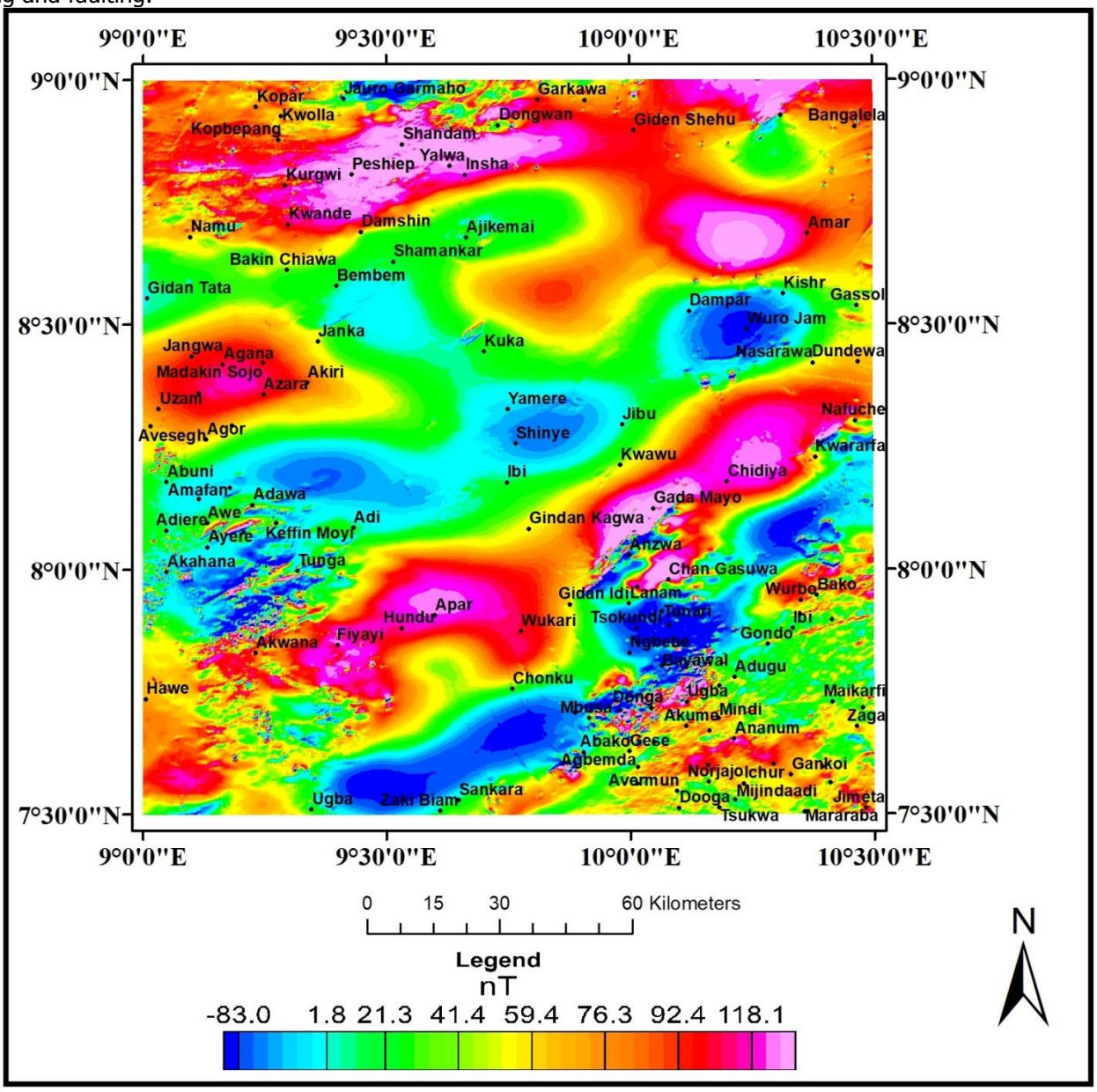

Figure 3.13: Residual Magnetic Intensity (RMI) Map of the Study Area

The Analytic signal filter was applied to the airborne residual magnetic intensity field data (RMI) to produce Figure 3.14. It sharpen the edge of bodies within the study area. Magnetic bodies are better interpreted within the analytic signal map. Folds and sills are observed around Yamere, Shinye, Dampar, Auro, Nasarawa Dundewa, Kishr and Gassol. Numerous longitudinal bodies trending NE-SW is also observed at Bangalala and Giden Shehu. Akwana and Fiyayi,

Chonku Akahana, Tunga, Keffin, Awe, Adiere areas is seen to have numerous magnetic bodies indicative to igneous rocks such as porphyritic granite. NW-SE trending structures is observed at Hawe, Hundu, Apar, Wukari, Chidiya, Chan Gasuwa and Kwararfa; while, Kopar, Jauro Garmaho, Peshiep, Kopbepand, Kurgwi, Shandam, Yalwa, Kwande, Namu, Anzwa, Chan Gasuwa, Wurbo, Bako, Gidan Idi, Tunari, Yerima Baya, Bako, Gbakpo, Ugba, Maikarfi, Zaga, Mindi, Mbusa, Zaki Biam, Avermun, Dooga, Mararaba and Gidan Usumanu is interpreted to be characterized my high amplitude magnetic bodies. High amplitude magnetic body trending NE-SW is also observed stretching from Janka to Bembem.

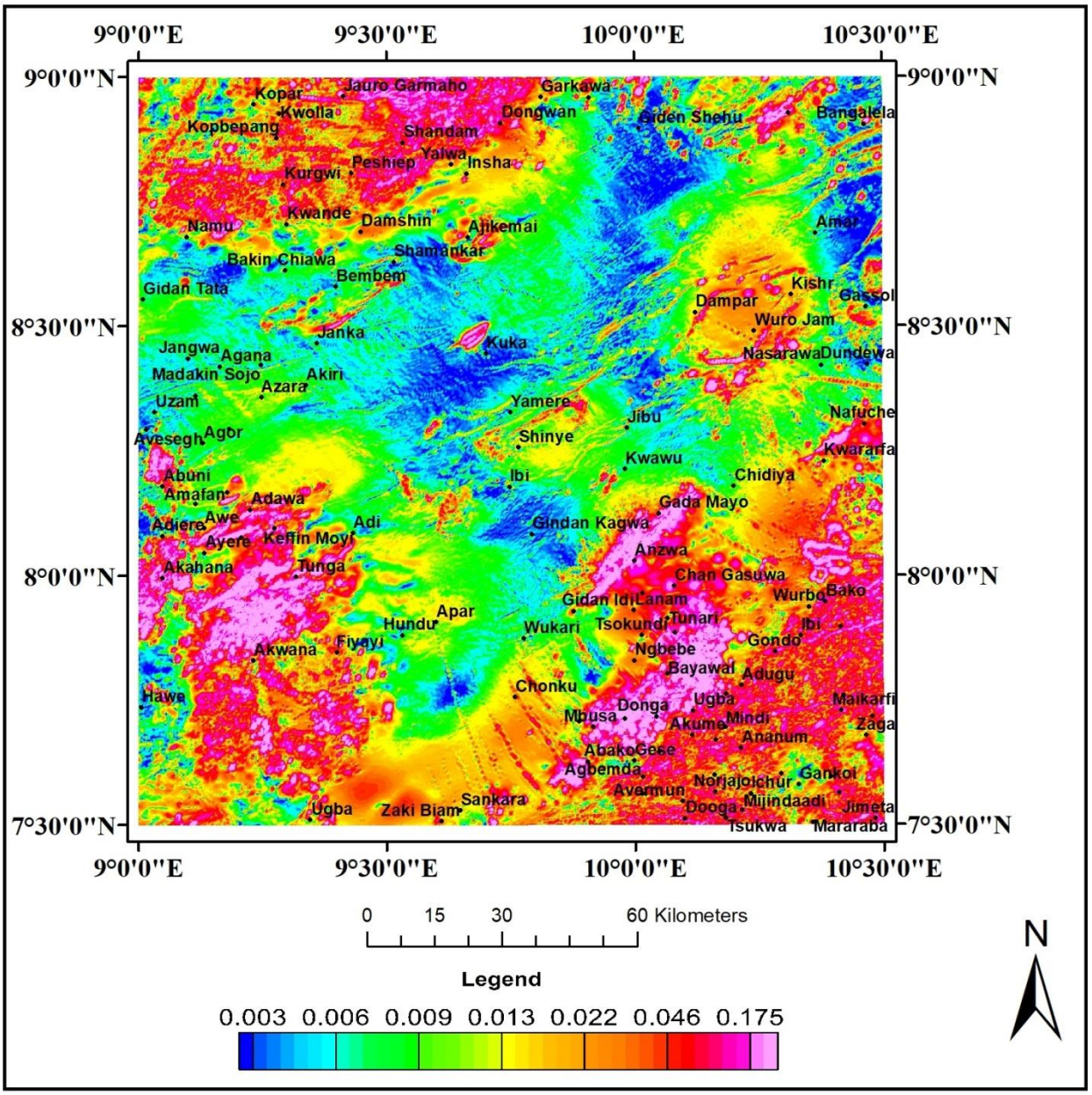

Figure 3.14: Analytic Signal Map of the Study Area

First vertical derivative filter removed long wavelength features of the magnetic field and significantly improved the resolution of closely spaced and shallow anomalies. Comparison of the first vertical derivative map (Figure 3.15), with the residual field map (Figure 4), shows an improved visibility of structural features such as faults, fractures and folds, within the first vertical derivative map structures are represented as bi-polar bodies. The folds around Dampar, Kishr, Wuro Jam and Nasarawa Dundewa as better visualized, the structures at Gindan Kagwa, Anzwa and Gadan Mayo with a NE-SW trend is also better enhanced for interpretation and mapping. The faults and fracture at Madakin Sojo, Uzam, Jangwa, Azara and Akiri, that were not visible in the analytic signal and residual map is also better mapped. NW-SE trending structures within Chonku – Wukari axis are also better interpreted and Bangalala, Amar and Ginden Shehu axis faults and fractures are also better visualized. The contact between the basement complex and sedimentary basin (Middle Benue Trough) is also better highlighted, trending NE-SW.

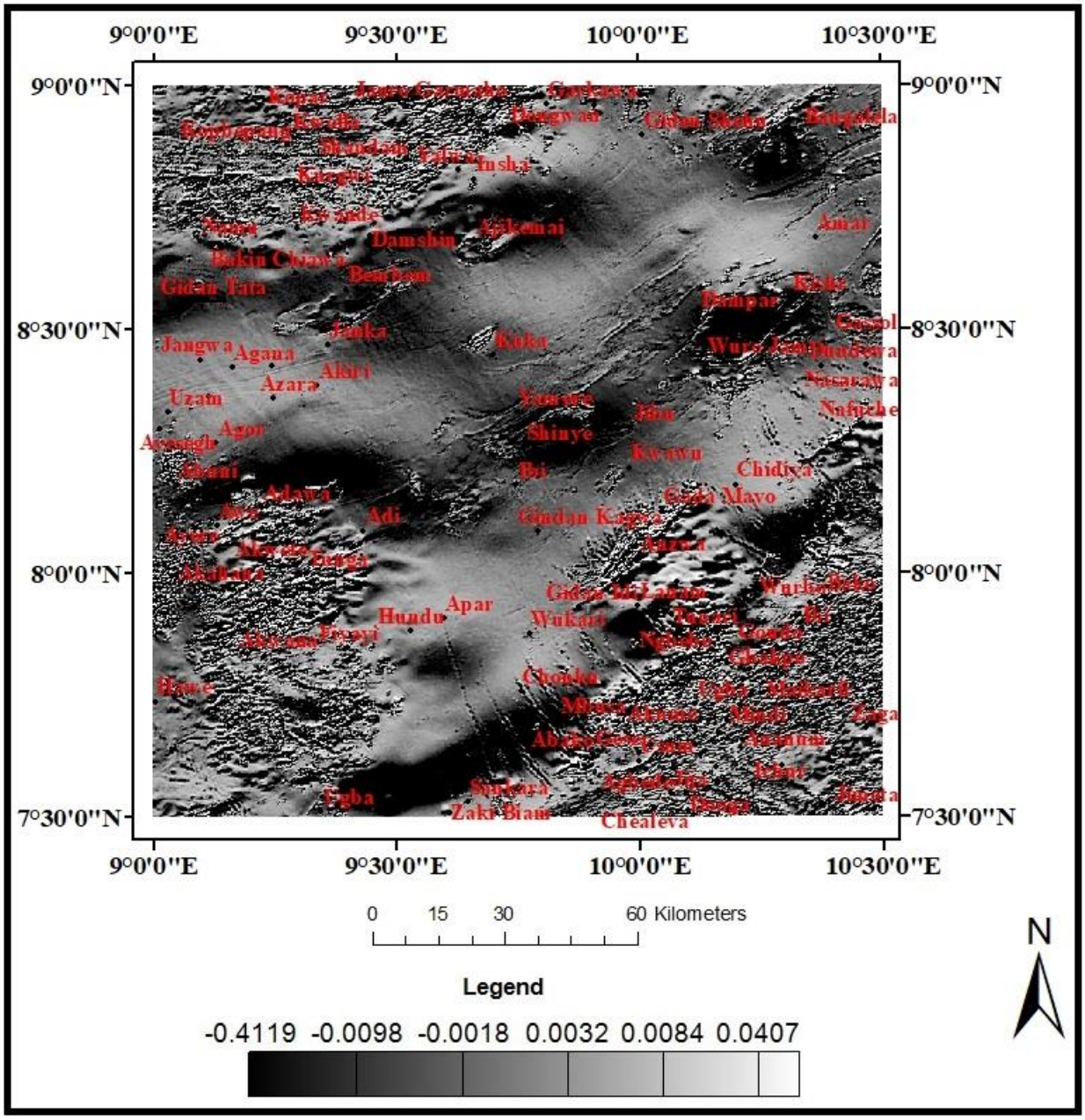

Figure 3.15: First Vertical Derivative Map of the Study Area.

These interpreted structures were used to generate a structural map of the study area (Figure 3.16). The structural map reflects a general NE-SW structural trend within the study area, with minor NW-SE and EW trending structures. The Central Benue trough is dominated by a series of NE-SW trending fractures and folds which are interpreted as high angle fault and fold structures formed during regional NW-SE compression resulting in a high degree of shearing and faulting at the contact zone, this is in agreement with the works of [15,1617,18,19,20,21,22]. The contact between the Central Benue Trough and Eastern Nigerian Massif is characterized by NW-SE trending structures and the Northern and Eastern Nigerian Massif within the study area is characterized by NE-SW and EW trending structures.

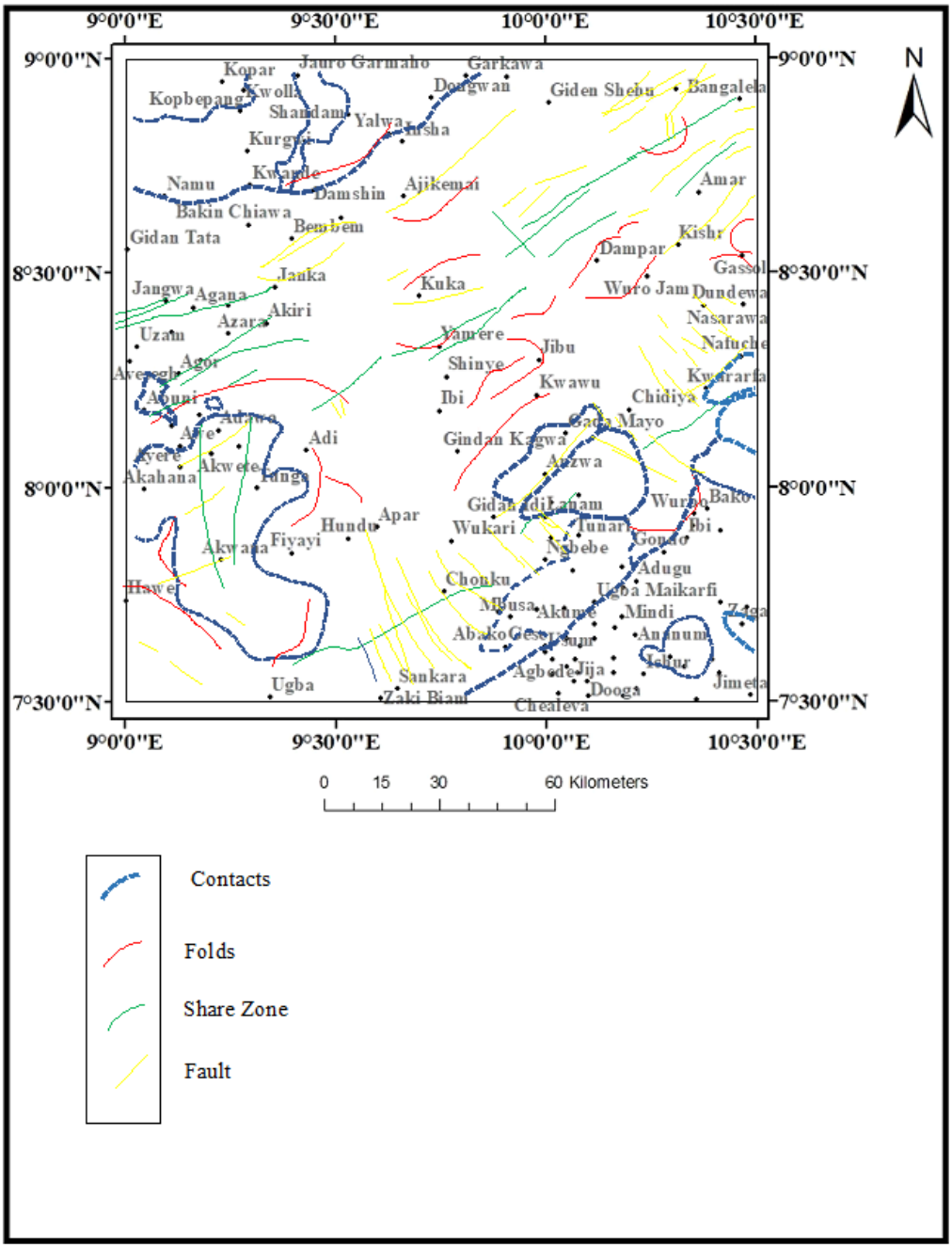

Figure 3.16: Interpreted Structural Map of the Study Area

In sandstone environment, mineralized areas are characterized by magnetic mineral enrichment in sediments due to feroginization, while in shale environment mineralized altered zone are characterized by destruction of magnetic minerals, all having intense structural activities which serves as conduit for mineral forming hydrothermal fluids (Kelma Geodynamics, 2019). Based on these principle, areas of high potential of hosting mineralized deposits in sandstone/shale environment include Wukari, Akwana, Chonku, Fiyayi, Apar, Bangalala, Chindiya, and Nafuche with preference to NW-SE structures, while at Bangalala, GidenShehbu and Amar structural preference is the NE-SW directional structures. The contact between sediment and Basement rock around Adiere, Ae, Adawa, Amafan, Aboni, Hawe and Adi also show good potential. The shale environment of interest is observed around Dampar, Kishr, Wuro Jam, Shinye, Yamere, Ibi, Ajikemai, Bembem, Gidan Tata and Janka. Lead and Zinc mineral deposit is currently been exploited in Akwana, Wukari and Bangalala area, therefore this research has defined other potential mineralized areas within the study area, these areas are highly recommended for ground truthing.

The interpreted geological map (Figure 3.17) from landsat 8 imagery and aeromagnetic dataset shows the geologic units, structures, deformation intensity and OH bearing, ferrumagnetisation and ferruginization alteration mapped.

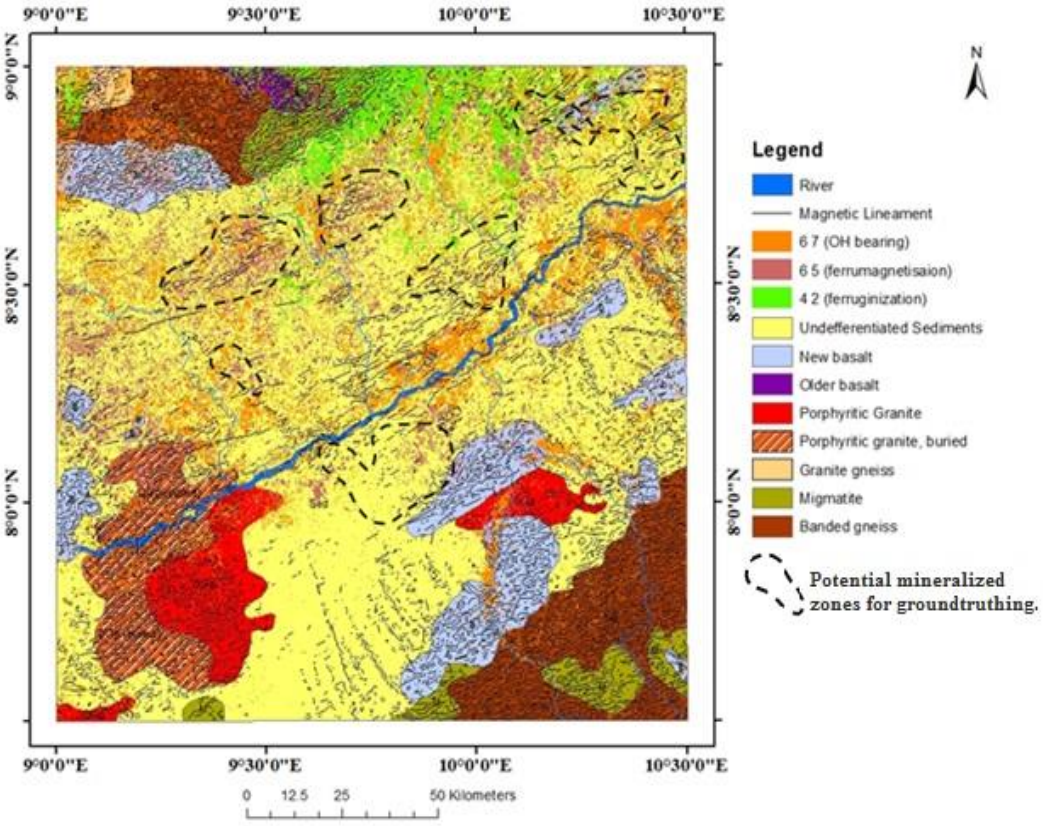

Figure 3.17: Interpreted geologic map from aeromagnetic and Landsat dataset [14]

4. CONCLUSION

From the Landsat imagery data processing and analysis, an alteration map was produced. The alteration map represents the map of thermally altered rocks in parts of the Middle Benue Trough. Aeromagnetic data covering parts of the Middlel Benue Trough was processed and filtered in other to validate the alteration map as well as to evaluate the mineral potential of the study area. Qualitative interpretation of the residual magnetic intensity was used to map magnetic depleted areas within the shales of the study area. These areas include Dampar, Wuro Jam, Kishr, Yamere and Shinye. The structures within the area shows a major NE-SW trend within the Middle Benue Trough and NW-SE structures at the contact between the Trough and Eastern Nigerian Massif, the longest with length of 42 km from Sankara to Apar, Hundu area. Hydrothermal zones observed in the alteration map coincide with a low magnetic amplitude stretching from Ugba to Kwarata, is interpreted as a previously active zones at the contact between the Middle Benue Trough and Eastern Nigerian Massief, this zone is interpreted as a major area of interest, especially around intense structurally active areas at Wukari, Chonku, Ngbebe, Bayawai, Gidan Idi, Wamgbe, Gusawa, Anzwa and Gada Mayo. Major folds are mapped at Dampar, Wuro Jam and Kishr area. Long stretched fault systems within the Middle Benue trough is observed at Bangalala, Gwinwan, Amar, Yamere and Rufai, Uzam, Sojo area. Integration of Landsat imagery, aeromagnetic interpretation and geological information defined Wukari, Akwana, Chonku, Fiyayi, Apar, Bangalala, Chindiya, Nafuche, Dampar, Kishr, Wuro Jam, Shinye, Yamere, Ibi, Ajikemai, Bembem, Gidan Tata and Jankaas area of highest potential of mineralization occurrences based on their geology, extensive alteration and structural complexity.

Acknowledgments: The authors would like to thank the Director General of Nigeria Geological Survey Agency (NGSA). Abuja, Mr. A. N Nwegbu for the postgraduate internship opportunity in the year 2018. And , the Head of Geophysics (NGSA), Mr. A. U Abba for the great impact and technical assistance in the cause of the postgraduate internship.

Conflicts of Interest: The authors declare no conflict of interest.

5. REFERENCE

1. Akande, S. O., Horn, E. E., & Reutel, C. Minerology, fluid inclusion and genesis of the Arufu and Akwana Pb-Zn mineralization, middle Benue Trough, Nigeria. *Journal of African Earth Sciences*. 1988; 7(1):167–180.
2. Oskouei, M.M., and Poormirzaee ,R. Estimation of virtual dimensionality of hyperspectral data by principle component analysis and higher order statistical method, *Proceedings of the 5th WSEAS International Conference on REMOTE SENSING,* Genova, Italy, 2009; p. 67-72.
3. King, L .C. Outline and disruption of Gondwanaland. *Geol. Mag*. 1950; 87: 353–359.
4. Stoneley, R. The Niger Delta region in the light of the theory of continental drift. *Geol. Mag*. 1966; 103: 385–397.
5. Wright, J. B. South Atlantic continental drift and Benue Trough. *Tectonophysics.* 1968; 6,301–310: 464–480.
6. Grant, N. K. South Atlantic, Benue Trough and Gulf of Guinea Cretaceous triple junction. *Bull. Geol. Soc. Am*. 971; 82: 2295–2298.
7. Burke, K. C., & Dewey, J. F. Two plates in Africa during the Cretaceous.*Nature*, Lond. 1974;249, 313–316.
8. Olade, M. A. (1978). Early Cretaceous basalt volcanism and initial continental rifting in Benue Trough, Nigeria. *Nature Lond.* 273,458–459.
9. Thiessen, R., Burke, K. C., and Kidd, W. S. F. African hotspots and their relation to the underlying mantle. *Geology.* 1979; *7*:263–266.
10. Mascle, J., Marinho, M., and Wannesson, J. The structure of the Guinean continental margins: Implications for the connection between the Central and the South Atlantic Oceans. *Geol. Rundsch*. 1986; 75: 57–70.
11. Benkhelil J. The origin and evolution of the Cretaceous Benue Trough (Nigeria). *J. African Earth Sci.* 1989;8: 251–282.
12. Nurnberg, D., and Muller, R.D. The tectonic evolution of the South Atlantic from Late Jurassic to present. *Tectonophysics.* 1991; 191: 27–53.
13. Offodile, M. E. The geology of the Middle Benue, Nigeria. Publications from the Palaeontological Inst. Of Univ. *Uppsala, Spec*. Pub. 1976; (4):166-178.
14. NGSA (2006). Lineament and Geological Map of Nigeria, Scale 1:100 000
15. Cratchley, C. R. a & Jones, G. P. (1965). An interpretation of geology and gravity anomalies of the Benue valley, Nigeria Geophysics Paper, Overseas Geol. Surv. London, 1: 1-26.
16. Ofoegbu, C. O. Aeromagnetic anomalies over the Lower and Middle Benue Trough, Nigeria. *J. Afr. Earth Sci.* 1984; 3: 293-2.
17. Charles, O.O. Interpretation of aeromagnetic anomalies over the Lower and Middle Benue Trough of Nigeria. *Geophysical Journal International.* 2007.
18. Obaje, N.G., (2009). Geology and Mineral Resources of Nigeria. *Springer Publishers*, Germany.
19.Nwosu, O. B. Determination of Magnetic Basement Depth over Parts of Middle Benue Trough by Source Parameter Imaging (SPI) Techniques using HRAM. *Int. J. Sc. Tech. Res.* 2014;3(1): 262-271.
20. Ugwu, C. M., Ugwu, G. Z. and Alasi, T. K. Spectral analysis and source parameter imaging of aeromagnetic anomalies over Ogoja and Bansara areas of Lower Benue Trough, Nigeria. *J. Geol. Min. Res*. 2018;10(13): 28-38.
21. Rowland A.A., and Nur, A. Interpretation of High Resolution Aeromagnetic Data for Hydrocarbon Potentials over Parts of Nasarawa and Environs North-Central Nigeria. *World Journal of Applied Physics. 2019*; 4(1): 1-11
22. Onyishi G.E., and Ugwu, G. Z. Source Parameter Imaging and Euler Deconvolution of Aeromagnetic Anomalies over Parts of the Middle Benue Trough, Nigeria. *American Journal of Geophysics, Geochemistry and Geosystems.* 2019;5(1): 1-9.
23. Nwajide, C. S. Geology of Nigeria's Sedimentary Basins. *CSS bookshops limited*. 2013; 290.
24. Luo, Y., Wang, M., Luo, F., & Tian, S. (2011). Direct Analytic Signal Interpretation Of Potential Field Data Using 2-D Hilbert Transform. *Chinese Journal of Geophysics* Vol.54, No.4, 2011, Pp. 551 – 559
25. USGS (2015a). M7.8-36 km EofKhudi, Nepal. http://earthquake. usgs.gov /earthquakes/ eventpage/us20002926#scientific_finitefault:us_us20002926
26. USGS(2015b).NetQuakes: Station KATNP_NQ_01, 25 April 2015. Available on: http://earthquake .usgs.ov/monitoring/netquakes/station/KATNP_NQ_01/20150425061138/.
27. Crosta, A. P., & Moore, J. McM. Enhancement of Landsat Thematic Mapper Imagery for Residual Soil Mapping in SW Minais Gerais State, Brazil: A Prospecting Case History in Greenstone Belt Terrain. Proceedings of the 7th (ERIM) Thematic Conference: *Remote Sensing for exploration geology*. Calgary. 1989; 2-6 Oct, pp: 1173-1187.

Cite this article: Adikwu Stephen Onum, Ibeneme Sabinus Ikechukwu, Okereke Chikwendu Njoku, Obioha Young Ezenwa, and Iduma Uche. INTEGRATION OF LANDSAT IMAGERY AND HIGH RESOLUTION AEROMAGNETIC DATA FOR HYDROTHERMAL ALTERATION MAPPING IN PARTS OF THE MIDDLE-BENUE TROUGH, NIGERIA. *Am. J. innov. res. appl. sci.* 2021; 12(6): 258-277.